Soft Matter

RSC Publishing

PAPER

View Article Online
View Journal | View Issue

Cite this: *Soft Matter*, 2013, **9**, 921

Physicochemical and rheological properties of a novel monoolein-based vesicle gel†

Ruggero Angelico,[a] Maura Carboni,[b] Sandrina Lampis,[b] Judith Schmidt,[c] Yeshayahu Talmon,[c] Maura Monduzzi[b] and Sergio Murgia*[b]

Received 25th September 2012
Accepted 6th November 2012

DOI: 10.1039/c2sm27215f

www.rsc.org/softmatter

The present paper deals with the preparation and characterization of an innovative vesicle-based gel composed of monoolein and lauroylcholine chloride. A number of vesicular formulations were prepared, in the range of 4–14 wt% of the dispersed phase, to investigate the system evolution from a dilute uni-lamellar vesicle dispersion to a vesicle lipid gel. Morphology, thermal stability up to 55 °C, and viscoelastic properties, along with the effect of acid diclofenac inclusion within the formulation, were evaluated by cryo-TEM, SAXS, and rheological measurements. Moreover, the nanostructure of the vesicle dispersion obtained upon gel dilution in water was assessed by cryo-TEM and SAXS, while DLS was used to monitor the formulation stability (size and ζ-potential). All the collected results lead to the conclusion that this new vesicle-based gel displays all the requirements needed for application in the pharmaceutical and cosmetic fields.

1 Introduction

Surfactants and polar lipids are amphiphilic molecules that have a natural tendency to self-assemble in water, giving rise to a wide range of nanostructures which embrace micelles, liquid crystals, emulsions and microemulsions. Among these systems, vesicles represent a class of self-assembled nanostructures that have a wide range of applications, such as cell membrane models, biocompatible drug or cosmetic delivery systems, nanoreactors, and material templates.[1] Notably, depending on the chemical composition, vesicles may or may not be a true equilibrium state. In the latter case, they must be considered as metastable (thermodynamically unstable) nanostructures endowed with high kinetic stability.[2] In spite of the number of articles devoted to this subject, so far, the issue of the thermodynamic or kinetic origin of the vesicles' stability is still a matter of debate.[3]

When the volume fraction reaches the critical value of 0.494 (the limit before hard sphere crystallization),[4] these bilayered nanostructures may originate viscous systems basically composed of densely packed vesicles, commonly termed vesicle gels. Prepared by high-pressure homogenization and mainly composed of small uni-lamellar vesicles, gels based on phospholipids (Vesicular Phospholipid Gels, VPGs) have been known since the early nineties.[5,6] It was shown that they can serve as sustained release systems for various low molecular weight drugs, especially in the field of anticancer treatments.[7,8] Importantly, it was recently demonstrated that VPGs may effectively work as a protein depot system, allowing for a prolonged release of erythropoietin.[9]

The VPG formulations are often proposed for topical drug delivery[10] and depot applications since they overcome the major disadvantage of using vesicles for localized applications, which is the liquid nature of the preparation. Indeed, desirable viscosity of vesicle dispersions is sometimes achieved by vesicle incorporation into polymeric gels[11,12] or using thickening agents such as cellulose derivatives.[13] Nevertheless, in these cases, structural modification of the self-assembled nanostructure may arise because of polymer–amphiphile interactions. Moreover, vesicle gels represent a suitable storage form of vesicles because conventional vesicles can be easily obtained upon dilution with water.

In a previous paper, a novel cationic liposome nanocarrier, obtained by combining two penetration enhancers, namely monoolein and lauroylcholine chloride, was presented.[14] Such a system, composed of small uni-lamellar vesicles endowed with low polydispersity and excellent stability, was proposed for topical drug delivery. Indeed, skin penetration and permeation tests showed that the formulation was able to deliver acid diclofenac into the viable epidermis.[15]

Bearing in mind the good performances shown by that system and its possible relevance to the field of topical drug delivery, this paper is devoted to the exploration of the morphological and the viscoelastic properties of a gel system

[a]*University of Molise (DIAAA) e CSGI, v. De Sanctis, I-86100 Campobasso (CB), Italy*

[b]*Department of Chemical and Geological Science, University of Cagliari, CNBS e CSGI, s.s. 554 bivio Sestu, I-09042 Monserrato, CA, Italy. E-mail: murgias@unica.it; Tel: +39 0706754453*

[c]*Department of Chemical Engineering, Technion – Israel Institute of Technology, Haifa 3200, Israel*

† Electronic supplementary information (ESI) available: Further SAXS experiments. See DOI: 10.1039/c2sm27215f

prepared by simply increasing the vesicles' dispersed phase of the monoolein/lauroylcholine-based formulations.

2 Experimental

2.1 Chemicals

Monoolein (MO, 1-monooleoylglycerol, RYLO MG 90-glycerol monooleate; 98.1 wt% monoglyceride) was kindly provided by Danisco Ingredients, Brabrand, Denmark. Lauroylcholine chloride (LCh) was from TCI Europe. Distilled water, passed through a Milli-Q water purification system (Millipore), was used to prepare the samples. Diclofenac free acid (DCFH) was obtained by acidic precipitation from a solution of sodium diclofenac purchased from Sigma-Aldrich (Milan, Italy). All substances were used without further purification. All concentrations are given in wt%.

2.2 VLG preparation

Vesicular lipid gels (VLG), empty or loaded with DCFH (1 mg g^{-1}), were obtained by dispersing a weighed amount of MO in aqueous solutions containing LCh using an Ultra-Turrax T10 (IKA) device, equipped with a S10N-5G dispersing tool working at 30 000 rpm for 10 minutes. VLG characterization was performed as a function of dispersed phase (MO + LCh, indicated as DP in the text below) content between 4 and 14 wt%. The sample volume was usually 3 mL. To obtain drug-loaded liposomes, DCFH was dissolved in the melted monoolein before Ultra-Turrax dispersion. All the samples were analyzed at least 48 h after their preparation.

2.3 Cryogenic-transmission electron microscopy (cryo-TEM)

Vitrified specimens were prepared in a controlled environment vitrification system (CEVS), at 25 °C and 100% relative humidity. A drop of the sample was placed on a perforated carbon film-coated copper grid, blotted with filter paper, and plunged into liquid ethane at its freezing point. The vitrified specimens were transferred to an Oxford CT-3500 cooling holder, and observed at 120 kV acceleration voltage in an FEI T12 transmission electron microscope at about −180 °C in the low-dose imaging mode to minimize electron-beam radiation-damage. Images were digitally recorded with a Gatan US1000 high-resolution CCD camera.

2.4 Dynamic light scattering (DLS) and zeta (ζ)-potential experiments

Particle size and ζ-potential determinations of the vesicles were performed with a ZetaSizer nano ZS (Malvern Instruments, Malvern, UK) at a temperature of 25 ± 0.1 °C. Samples were backscattered by a 4 mW He–Ne laser (operating at a wavelength of 633 nm) at an angle of 173°. At least 2 independent samples were taken, each of which was measured 3–5 times.

2.5 Small angle X-ray scattering (SAXS)

Small-angle X-ray scattering was recorded with a S3-MICRO SWAXS camera system (HECUS X-ray Systems, Graz, Austria). Cu Kα radiation of wavelength 1.542 Å was provided by a GeniX X-ray generator, operating at 50 kV and 1 mA. A 1D-PSD-50 M system (HECUS X-ray Systems, Graz, Austria) containing 1024 channels of width 54.0 μm was used for the detection of scattered X-rays in the small-angle region. The working q-range ($Å^{-1}$) was $0.02 \leq q \leq 0.4$, where $q = 4\pi\sin(\theta)\lambda^{-1}$ is the modulus of the scattering wave vector. Experiments were performed using thin-walled 2 mm glass capillaries for liquid samples and a stainless steel sample holder with thin polymeric sheet (Bratfolie, Kalle) windows for viscous samples. The diffraction patterns were recorded for at least three hours. The solvent background scattering was subtracted from the intensity, and the resulting quantity was normalized and denoted as $I(q)$. To minimize scattering from air, the camera volume was kept under vacuum during the measurements. Silver behenate (CH_3–$(CH_2)_{20}$–COOAg) with a d spacing value of 58.38 Å was used as a standard to calibrate the angular scale of the measured intensity. SAXS patterns of uni-lamellar vesicle samples were analyzed in terms of a global model using the program GAP (Global Analysis Program). This technique models the full q-range in the SAXS regime including Bragg peaks and diffuse scattering. The electron density profile can be modelled by the summation of 3 Gaussian distributions, two centred at the position of the electron-dense lipid head groups ($\pm z_H$) and a third, of negative amplitude, in the middle of the bilayer, where the hydrocarbon chains meet. The corresponding standard variation widths of the Gaussians are given by σ_H and σ_C, respectively. The membrane thickness (d_B) was obtained by using the formula $d_B = 2(z_H + 2\sigma_H)$, where z_H was derived from the SAXS curve fitting with GAP.[16,17]

2.6 Rheology

Rheological analyses were performed in triplicate using a stress control rheometer (MARS III Thermo Haake Scientific) equipped with a cone–plate geometry and cone–plate angle 1° (gap 53 μm with diameters 20 mm and 60 mm, respectively, depending on the sample viscosity) operating in both steady and oscillation mode. The selected temperatures of 25 and 32 °C were controlled by the Peltier device with an accuracy of ± 0.1 °C. To prevent evaporation of water, the cone–plate cell was covered by a solvent trap. Steady state stress sweep experiments were carried out in both control stress and control rate mode to investigate the flow curves for several samples in the DP range of 4–14 wt%. For each flow curve, zero-shear viscosity was checked at low shear rates to determine the corresponding Newtonian plateau region.

For the dynamic oscillatory rheology investigation the samples were exposed to increasing stress (0.01–100 Pa) at a constant frequency (f = 0.1 or 1 Hz) to determine the linear viscoelastic range of the samples. Then, selected stress values in the linear region (usually 1–10 Pa) were used in the other oscillation tests.

In oscillatory frequency sweep experiments the samples were exposed to a stepwise increase in frequency (f = 0.01–100 Hz range) at a constant stress in the field of linear viscoelasticity. The frequency range (expressed in terms of angular frequency $\omega = 2\pi f$) and the shear storage (elastic) G' and loss (viscous) G'' moduli, both in Pa, were plotted on a logarithmic-linear scale.

Graphical data were reported as the mean of the three curves obtained from the repetitions.

3 Results and discussion

3.1 From vesicles to vesicle gel and back

A series of vesicle-based dispersions were prepared with a fixed ratio of MO/LCh and an increasing amount of the dispersed phase (MO + LCh), indicated as DP, from 4 up to 14 wt%. Samples were prepared by simply dispersing the components (MO and LCh) in water using an Ultra Turrax device as described in the Experimental section. Sample compositions and their macroscopic flow behavior are reported in Table 1.

All samples appeared bluish, while macroscopic viscoelastic behaviour changed from a low-viscous liquid to a not-flowing gel-like system as a function of DP content. The samples' nanostructure was evaluated *via* SAXS. Some representative SAXS patterns are reported in Fig. 1.

As can be seen, increasing the fraction of DP results in the appearance of quasi-Bragg peaks in the scattering curve. DP4 exhibited a pure diffuse scattering curve, while DP6 and DP12 showed low resolved peaks that can be attributed to an increase in the lamellarity of the system. Finally, DP14 scattering curve is characterized by the presence of three quasi-Bragg peaks. The SAXS profile clearly indicates the formation of aggregates with an oligo- or a multi-lamellar structure. The average interbilayer distance between adjacent bilayers (d_{av}), corresponding to 20 ± 3 nm, was calculated by using the Bragg relation $d_{av} = 2\pi h/q$, where q is the position of the various quasi-Bragg peaks and h is the Miller index.

The morphology of the DP14 vesicular gel was observed by transmission electron microscopy at cryogenic temperature (cryo-TEM).

In agreement with SAXS results, the cryo-TEM image reported in Fig. 2 shows that the most concentrated formulation (DP14) is composed of closely packed vesicles possessing an oligo-lamellar structure (OLV). In addition, the interbilayer distance (d) obtained by the image analysis was found to be 21 ± 4 nm, in conformity with the value (20 ± 3 nm) obtained through SAXS. It is worth recalling here that the formation of oligo- or multi-lamellar vesicles usually occurs in systems initially constituted by diluted uni-lamellar vesicles when the DP concentration is increased. Indeed, although vesicle shrinking and lamellar phase formation represent alternative morphological evolution pathways, the development of multi-walled vesicles represents the most convenient way in which these kinds of systems may arrange the additional interfacial area.[18] In other words, upon increasing the DP content the number of uni-lamellar vesicles increases until they approach a critical effective volume fraction. Once this threshold is reached, multi-walled vesicles may start forming in order to achieve a more densely packed configuration. Furthermore, nanostructures observed in Fig. 2 appear as circular or, sometimes, peanut-like concentric bilayers. Deviations from the spherical shape are commonly observed in VLG

Table 1 Sample composition and macroscopic behaviour

Sample	MO/LCh/W (wt%)	Macroscopic behaviour
DP4	3.3/0.3/96.4	Sol
DP6	5.1/0.5/94.4	Sol
DP8	7.0/0.6/92.4	Sol
DP9	7.9/0.7/91.4	Low viscous gel
DP10	8.8/0.8/90.4	Low viscous gel
DP12	10.6/1.0/88.4	High viscous gel
DP13	11.9/1.1/87.0	High viscous gel
DP14	13.2/1.2/85.6	Stiff gel

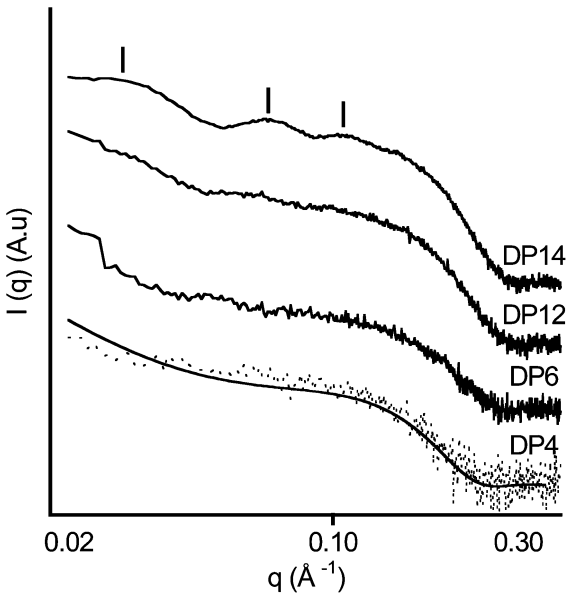

Fig. 1 log–log plot of SAXS patterns collected at 25 °C of the samples DP4, DP6, DP12, and DP14. Curves are shifted for clarity with multiplication factor 5. The dotted line in DP4 represents the experimental curve with the superimposed fitting curve (continuous line) obtained with GAP analysis.

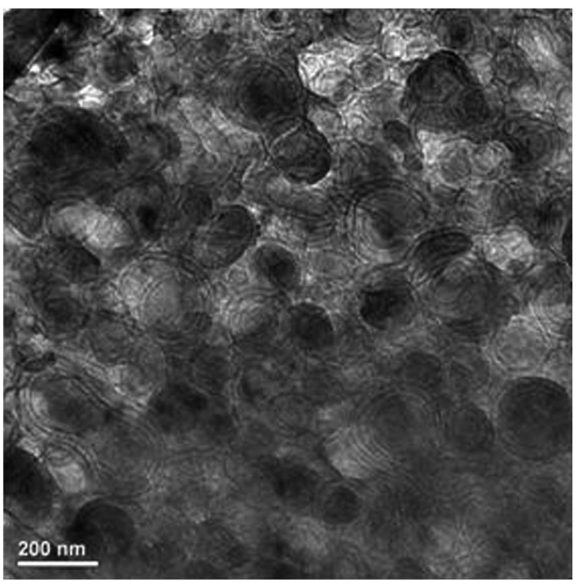

Fig. 2 Cryo-TEM image of the VLG sample DP14 with composition MO/LCh/W = 13.2/1.2/85.6 (wt%) showing oligolamellar close-packed vesicles.

systems, since also distorted morphologies allow for a better vesicle accommodation.[4]

VLG can be regarded as an easy way to store vesicles for a subsequent application, such as systemic use. Indeed, upon a simple VLG dilution, the spontaneous formation of small unilamellar vesicles (SUVs) often occurs. Therefore, to test the possibility that upon increasing the water content SUVs are formed also in the system under investigation, the DP14 VLG was diluted with water while a gentle shaking was applied for a few minutes. The resulting vesicle dispersions, which contained about 4 wt% of the dispersed phase, were re-investigated by SAXS, cryo-TEM and DLS for nanostructure, morphology and long-term stability. The SAXS profile, reported in Fig. 3 and superimposed on that of DP4, shows the typical diffuse scattering pattern of single, non-interacting bilayers.

The marked difference in the Guinier part of the two SAXS patterns evidenced that the particle size is dependent on the preparation pathway, showing that these vesicular aggregates are not the equilibrium state for this system. To shed some more light on the colloidal stability of the vesicles investigated in this work, the sample DP4 was newly prepared by mixing MO and LCh in water through a vortex mixer. In a couple of days such a system phase separated. This simple experiment has profound consequences. Indeed, since the property of being formulated by mixing the components without energy input is a fundamental requisite displayed by thermodynamically stable vesicle systems, the formerly reported experiment definitely proved that the system under investigation, although endowed with a very long shelf-life, is only kinetically stable.

The bilayer thickness d_B calculated with GAP (see the Experimental section) of the diluted VLG was found to be equal to 47 ± 1 Å, in agreement with previously reported data.[15] In Fig. 4 the micrograph of this sample is reported. Uni-lamellar vesicles dominate the sample, although some tubular vesicles are also present (not shown). From the rheological point of view this sample is identical to the sample DP4. Dilute VLG were monitored by DLS for 6 months to check formulation stability. Freshly prepared vesicles are characterized by a particle size distribution having an average diameter (D_{av}) of 79 nm and a polydispersity index (PI) of 0.277. One month old samples did not show any change in both D_{av} and PI, but 6 months after preparation these two parameters increased up to 94 nm and 0.430 respectively. ζ-Potential values remained around +60 mV over the entire period.

The thermal stability of the DP14 formulation was assessed *via* SAXS measurements performed at 25, 32 and 55 °C. The scattering patterns are shown in Fig. S1.† Particularly, the diffraction pattern at the highest temperature demonstrated the persistence of the nanostructure order and, compared to the system at 25 °C, a slight (1 nm) decrease of d was observed due to thermal fluctuations.

Given the potential application of this VLG system as a drug carrier, the ability to host molecules of pharmaceutical interest was tested by entrapping 1 mg g^{-1} of diclofenac in its acid, hydrophobic form (DCFH). Compared to the formulation not carrying the drug, the latter showed an almost identical SAXS pattern (see Fig. S2†). It can therefore be concluded that the vesicle's hydrophobic compartment can suitably accommodate the DCFH drug without losing the original nanostructure.

3.2 Rheological characterization of VLG

The rheological behavior of a dispersion of vesicles depends on the interaction between vesicles and the vesicle deformability.[19] In vesicle based systems, because of the great amount of solvent vesicles encapsulate in their interior, the effective volume fraction ϕ_v is much larger than the nominal surfactant ϕ_s contained in vesicle bilayers. As a result, even at extremely low DP, in such systems vesicles are densely packed and a highly viscous behavior and (possibly) a yield stress are observed, indicating a gel-like behavior.[20]

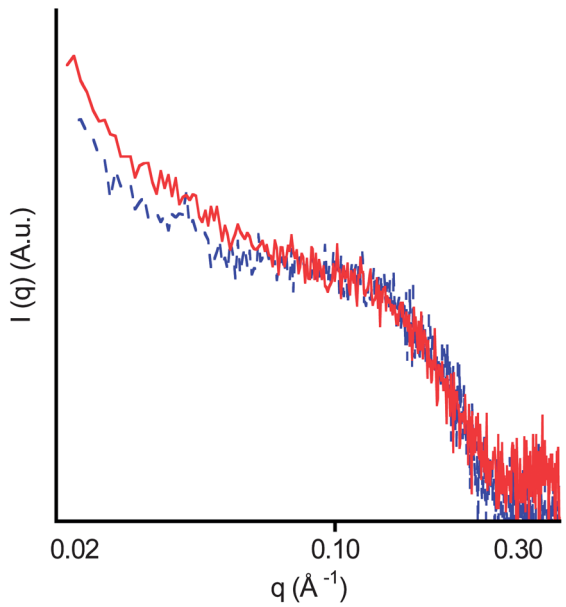

Fig. 3 log–log plot of SAXS patterns collected at 25 °C of the VLG diluted sample (dashed line) of composition MO/LCh/W = 3.3/0.3/96.4 (wt%) compared with the DP4 sample (solid line) having the same nominal composition.

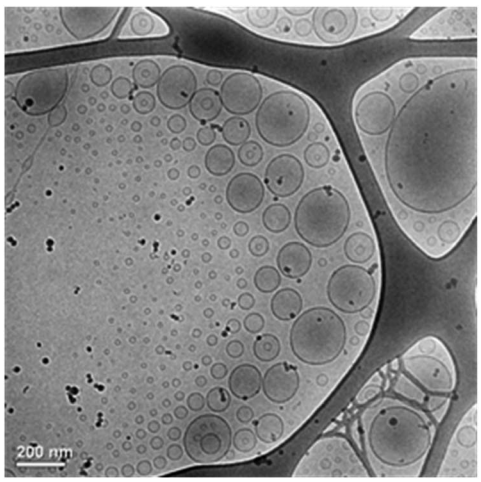

Fig. 4 Cryo-TEM images of the sample MO/LCh/W 3.3/0.3/96.4 (w/w%) obtained from dilution of VLG (DP14).

To understand the effect of the deformation of the VLG induced by the shear forces, steady state flow curves in terms of dynamic viscosity η *vs.* shear rate $\dot{\gamma}$ were obtained as a function of the total DP in the range of 4–14 wt%. Rheograms were also obtained for the model drug delivery system formulated with DCFH. Differently from the sample at the lowest DP content (4 wt %), which is characterized by a constant value of viscosity ($\eta = 9.7 \pm 0.4$ mPa s) over a wide range of shear rate (Newtonian liquid), formulations prepared at the higher DP content showed a non-linear behavior typical of non-Newtonian pseudoplastic fluids. Indeed, above a certain threshold shear rate, η decreases as $\dot{\gamma}$ increases. This phenomenon, the so-called shear-thinning, is rather common in oligo- and multilamellar vesicle systems.[21] A widely accepted concept is that at low ϕ_v vesicles relax the external stress through simple Brownian motion by changing particle position distribution. However, the cryo-TEM images of more concentrated samples show oligo-lamellar organization for densely packed vesicles (see Fig. 2). Thus a possible physical reason for the shear thinning observed in the steady-state shear viscosity experiments at higher DP is that on increasing the shear rate the outer shells of oligo-lamellar vesicles may be stripped off, thereby leading to smaller vesicles that do not contribute much to the system's viscosity.[22] Other reasonable explanations can be invoked. Particularly, vesicular structures can be deformed during shearing and/or randomly distributed vesicles can come in alignment during shearing. Thus, though dilute vesicle solutions can be treated as hard-sphere dispersions, at moderate to high concentrations the response to mechanical stress can assume the properties of viscoelastic gels near $\phi_v^* = 0.74$ (the maximum packing fraction for spheres). However, at very low shear rates, a region may exist where viscosity remains constant even for non-Newtonian systems, usually defined as zero-shear viscosity η_0.[23] At very high shear rates, viscosity may become constant again, giving rise to a behavior known as limiting viscosity at infinite shear η_∞. Among the various models useful to describe the shear-thinning behavior of most of the complex systems, the Cross equation[24] can be invoked to interpret the flow curves observed in the system under investigation:

$$\frac{\eta_0 - \eta}{\eta - \eta_\infty} = (K\dot{\gamma})^m \quad (1)$$

The dimensionless parameter m is known as the (Cross) rate constant, which is a measure of the degree of dependence of viscosity on shear rate in the shear-thinning region. A value of zero for m indicates Newtonian behaviour, with $m \to 1$ for increasingly shear thinning behaviour. K is known as the (Cross) time constant (or, sometimes, as the consistency) and has the dimension of time. The reciprocal, $1/K$, gives a critical shear rate, a useful indicator of the onset shear rate for shear thinning.

In the limit $\eta \gg \eta_\infty$ eqn (1) can be reduced to the following expression:

$$\eta(\dot{\gamma}) = \frac{\eta_0}{1 + (K\dot{\gamma})^m} \quad (2)$$

Fig. 5 shows the log–log plot of the flow curves for several DP values together with the best non-linear fits of eqn (2), while in

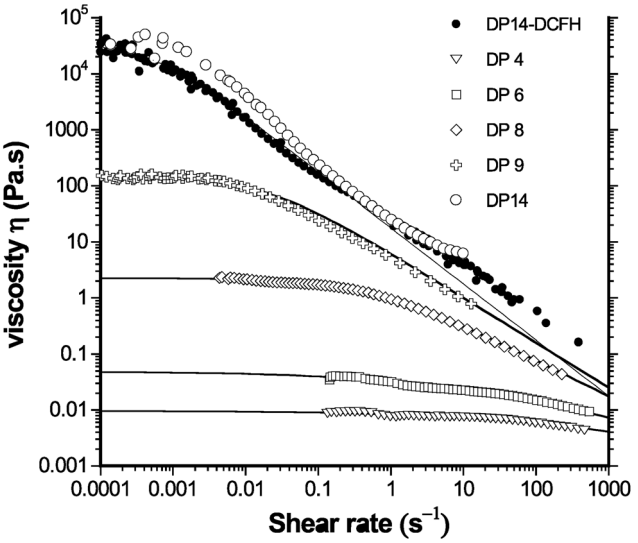

Fig. 5 log–log plot of shear viscosity *vs.* shear rate measured in steady state experiments as a function of DP. The solid lines are the best fits of eqn (2).

Table 2 Best non-linear fits of the Cross equation

DP (wt%)	η_0 (Pa s)	K (s)	m
4	0.0097 ($\pm 4 \times 10^{-4}$)	0.0027 ($\pm 5 \times 10^{-4}$)	0.31 ($\pm$0.04)
6	0.049 ($\pm 1 \times 10^{-3}$)	0.14 ($\pm$0.02)	0.35 ($\pm$0.05)
8	2.28 ($\pm$0.02)	1.75 ($\pm$0.09)	0.65 ($\pm$0.08)
9	150 ($\pm$2)	52 ($\pm$6)	0.8 ($\pm$0.1)
10	5300 ($\pm$300)	850 ($\pm$84)	1.10 ($\pm$0.05)
12	8500 ($\pm$350)	3360 ($\pm$320)	1.06 ($\pm$0.04)
14	37×10^3 ($\pm 2 \times 10^3$)	396 ($\pm$77)	1.3 ($\pm$0.2)
DCFH	36×10^3 ($\pm 1 \times 10^3$)	2025 ($\pm$200)	1.0 ($\pm$0.1)

Table 2 the fitting parameters are summarized for the explored compositions. As can be noticed from the listed parameters, the vesicle gel loaded with DCFH starts flowing at lower shear rates (1/2025 $s = 5 \times 10^{-4}$ s^{-1}) than the corresponding empty system DP14 (1/396 $s = 2.5 \times 10^{-3}$ s^{-1}), implying that the former gel is more prone to flow than the latter. This is in accord with a decrease of storage modulus G' observed for DP14 loaded with DCFH compared to DP14 (see Fig. 7 and 8) and with the presence of less deformable (hence, worse packed) vesicular aggregates. On the other hand, considering the statistical errors associated with the fitted parameters, both the systems share the same m values, while equal values for η_0 indicate that the material properties are roughly the same in the regime of shear tending to zero, *i.e.*, in regimes of no deformations.

The zero-shear viscosity dependence on the vesicle composition can be appreciated by plotting η_0 *vs.* DP as in Fig. 6.

Gel-like structures, such as particle gels or colloidal glasses, are basically found under conditions where either repulsive or attractive interactions dominate. For example, concerning ideal hard-sphere particles, the transition from a liquid to a disordered solid phase – a glass – can be observed at volume fractions of about $\phi \approx 0.58$.[25] Most of the sol–gel transitions occur

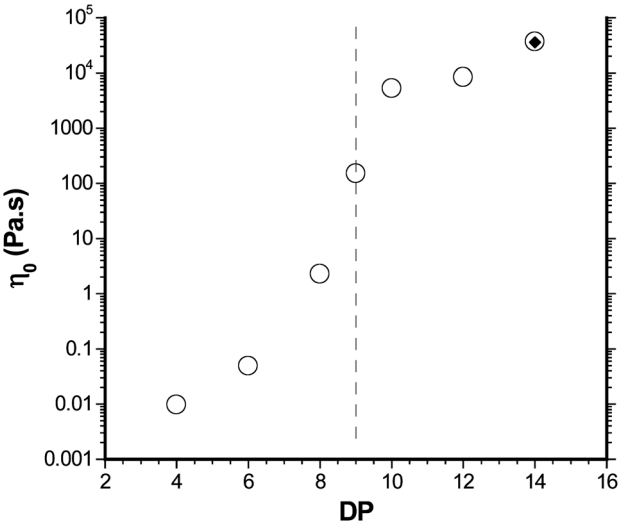

Fig. 6 Semi-log plot of zero-shear viscosity η_0 as a function of DP. The closed rhombus corresponds to the sample DP14 formulated with DCFH. The vertical dashed line indicates a rough transition between sol- and gel-vesicle systems.

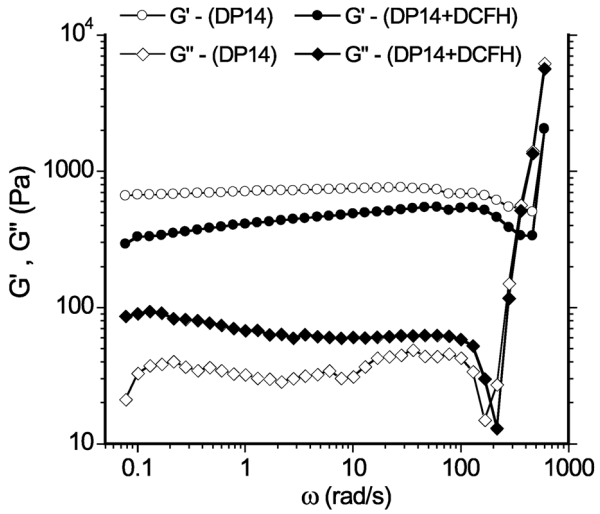

Fig. 7 Linear viscoelastic experiments at 25 °C for DP14 sample (open symbols) and DP14 sample loaded with diclofenac DCFH (closed symbols). Circles: storage modulus G'; diamonds: loss modulus G''.

through the formation of an interconnected fractal-like network of colloidal particles, which results in a soft viscoelastic solid, known as a gel state.[26] From the rheological data shown, the onset of vesicle gelation can be identified in correspondence with the onset of shear-thinning behavior, when m approaches unity. This represents the hallmark of a densely packed system of vesicles. Above this threshold concentration, a dynamical arrest (jamming or gelation) is frequently encountered in colloidal suspensions.[27,28] In the system under investigation, such a situation is met near DP 9 wt% (see Fig. 6), when vesicles' mobility is hindered owing to repulsive forces coming from the close presence of neighboring particles. When the surfactant content exceeds DP 9 wt%, oligo-lamellar structures form, as revealed by SAXS (Fig. 1) and cryo-TEM (Fig. 2). Once these samples undergo shear flow, the oligo-lamellar vesicles may strip off and a shear-thinning behaviour can be observed. On the contrary, below DP *ca.* 9 wt% (uni-lamellar) vesicles can relax the imposed stress through Brownian motions, which is the typical response of Newtonian liquids. Of course, the sol–gel transition is not really sharp and a continuous transition from Newtonian (Cross parameter $m < 1$) to pseudo-plastic behavior ($m \approx 1$) can be observed.

Linear viscoelastic measurements in the oscillatory mode showed a near-Maxwell behaviour at low DP, characterized, in the low frequency range, by higher viscous G'' than elastic G' modulus (data not shown). The opposite holds in the high frequency regime. On increasing the DP content the viscoelastic properties of the more densely packed OLV showed $G' > G''$ (Fig. 7, open symbols), both the moduli being almost frequency independent in the entire frequency range (at least below 200 rad s^{-1}). The effect of dispersing DFCH into vesicle bilayers is reflected in a significant decrease of G' and a concomitant increase of G'' (Fig. 7, closed symbols). In addition, the G' dependence on DP is more marked at higher DP values. This means that when approaching the maximum packing fraction,

Table 3 Storage (G') and loss (G'') moduli (in Pa) at 10 Hz obtained at 25 and 32 °C as a function of the dispersed phase DP

	25 °C		32 °C	
DP (wt%)	G' (Pa)	G'' (Pa)	G' (Pa)	G'' (Pa)
9	91 (±18)	25.7 (±0.8)	75 (±12)	23.0 (±1.5)
10	213 (±47)	19.8 (±3.5)	204 (±46)	23.6 (±3.9)
12	193 (±30)	36.1 (±9.5)	257 (±40)	32.5 (±4.8)
13	365 (±47)	63.4 (±9.2)	319 (±36)	62.5 (±8.9)
14	733 (±50)	69.0 (±9)	532 (±50)	58.0 (±5)
DCFH	582 (±53)	76 (±18)	517 (±45)	90 (±10)

vesicle interaction and deformability can make an important contribution to the storage modulus G'.[29] Differently, the complex viscosity is strongly frequency dependent and decreases as the frequency increases with a slope equal to −1 (data not shown). Table 3 reports, at 25 and 32 °C, the measured G' and G'' moduli at 10 Hz as a function of DP. G' data are also displayed in Fig. 8, which illustrate a non-linear dependence of the storage modulus *vs.* DP.

In vesicle systems G' is inversely proportional to the cubic power of the vesicle radius.[19] Consequently, the highest G' value observed in Fig. 8 somehow reflects the vesicles packing compatible with the vesicle sizes and deformability at DP = 14 wt%. Therefore, the drop of G' observed in the presence of DCFH at $T = 25$ °C (see Fig. 8) may indicate that drug encapsulation originates larger and less deformable (hence, worse packed) vesicular aggregates. In turn, this suggests that entrapment of DCFH within the bilayer provokes an increase in the elastic bending modulus k_c of the lipid membrane, giving rise to more rigid films akin to the well known effect observed for cholesterol.[30] Such hypothesis is supported by the huge increase in the vesicles' size (from about 80 to 200 nm) previously reported when a formulation of composition identical to DP4 was loaded with DCFH.[15] The previous arguments are

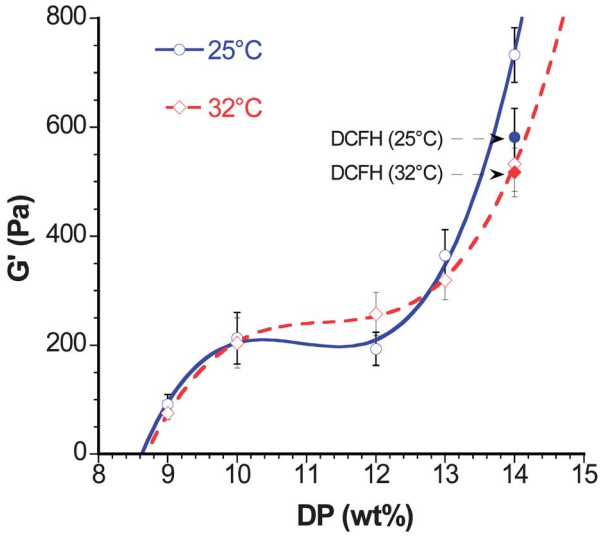

Fig. 8 Storage modulus G' as a function of DP compositions at two different temperatures. $T = 25$ °C: open circles with the solid line as guide for eyes; the closed circle corresponds to DP14 gel vesicles encapsulating DCFH. $T = 32$ °C: open diamonds with the dashed line as guide for eyes; the closed diamond corresponds to DP14 gel vesicles encapsulating DCFH.

consistent with the dependence of G' on temperature. Indeed, owing to the expected result that k_c decreases as temperature increases,[31] the slight increment of T (from 25 to 32 °C, see Fig. 8) has a greater effect on the more flexible bilayers of empty vesicles compared to the analogous system loaded with DCFH, leading finally to $G' \approx G'_{DCFH}$ at DP 14 wt%. Finally, it deserves noticing that the drop of G' observed in the DP14 sample loaded with DCFH should result in a strong variation of the quasi-Bragg peaks' width. Nevertheless, because of the diffuse scattering superimposed on the SAXS patterns, the Caillé analysis[32] was not practicable (see Fig. S2†).

4 Conclusions

Throughout this paper a novel vesicle gel formulation endowed with very high kinetic stability was presented and its morphological and viscoelastic features were discussed. It was previously observed that the (cationic) lauroylcholine chloride, intercalated within the (non-ionic) monoolein palisade, modifies the monoolein effective packing parameter, decreases the bilayer rigidity and allows for its folding towards vesicle formation.[14] Here, it was demonstrated that, starting from such a formulation and increasing the dispersed phase DP content at a constant monoolein/lauroylcholine chloride ratio, a vesicular lipid gel can be obtained. Above a DP threshold, a transition from a sol- to gel-vesicle system has been found through linear viscoelastic experiments. SAXS and cryo-TEM results showed that the most concentrated formulation (DP14) is composed of closely packed vesicles possessing an oligo-lamellar structure (OLV), and both the techniques yielded a similar interbilayer distance ($d = 21$ nm and 20 nm, from cryo-TEM and SAXS, respectively). The thermal stability of the formulation with the highest concentration was assessed *via* SAXS measurements performed at 25, 32 and 55 °C. Upon water dilution of concentrated vesicle dispersions the nanostructure of the resulting aggregates, containing about 4 wt% of DP, was re-investigated by SAXS, cryo-TEM and DLS to check morphology and long-term stability. All these techniques confirmed that the vesicle solution obtained by dilution is very similar to that prepared by simply dispersing monoolein and lauroylcholine chloride in water at the same concentration. Rheological results showed a typical shear-thinning behavior observed in the majority of vesicle dispersions.

In particular, the analysis of the dynamic elastic modulus suggested that the inclusion of hydrophobic acid diclofenac into the lipid bilayer can lead to an increased film rigidity.

Within the panorama of vesicular gels, it should be highlighted that the preparation of the gel system here described is easy and very fast, and does not require high-pressure homogenization or organic solvents. These are a number of important points in view of a possible scale-up. Moreover, the elastic rheological response of densely packed vesicles (vesicle gels), combined with the shear-thinning effect, may rapidly result in a commercially available product valuable in the pharmaceutical and cosmetic fields.

Notes and references

1 C. Oppel, S. Prevost, L. Noirez and M. Gradzielski, *Langmuir*, 2011, **27**, 8885–8897.
2 E. F. Marques, *Langmuir*, 2000, **16**, 4798.
3 L. Tayebi, D. Vashaee and A. N. Parikh, *ChemPhysChem*, 2012, **13**, 314–322.
4 M. Gradzielski, *J. Phys.: Condens. Matter*, 2003, **15**, R655.
5 M. Brandl, D. Bachmann, R. Reszka and M. Drechsler, *US Pat.* 6,399,094, 2002.
6 M. Brandl and R. Reszka, *Proc. Int. Symp. Controlled Release Bioact. Mater.*, 1995, 472–473.
7 N. Kaiser, A. Kimpfler, U. Massing, A. M. Burger, H. H. Fiebig, M. Brandl and R. Schubert, *Int. J. Pharm.*, 2003, **256**, 123–131.
8 N. Qi, X. Tang, X. Lin, P. Gu, C. Cai, H. Xu, H. He and Y. Zhang, *Inter. J. Pharm.*, 2012, **427**, 234–241.
9 W. Tian, S. Schulze, M. Brandl and G. Winter, *J. Controlled Release*, 2010, **142**, 319–325.
10 C. Puglia, D. Trombetta, V. Venuti, A. Saija and F. Bonina, *J. Pharm. Pharmacol.*, 2010, **56**, 1225–1232.
11 M. Carafa, C. Marianecci, L. Di Marzio, F. Rinaldi, C. Di Meo, P. Matricardi, F. Alhaique and T. Coviello, *J. Pharm. Pharm. Sci.*, 2011, **14**, 336–346.
12 M. Foldvari, *J. Microencapsulation*, 1996, **13**, 589–600.
13 Z. Pavelic, N. Skalko-Basnet, J. Filipovic-Grcic, A. Martinac and I. Jalsenjak, *J. Controlled Release*, 2005, **106**, 34–43.
14 S. Murgia, A. M. Falchi, M. Mano, S. Lampis, R. Angius, A. M. Carnerup, J. Schmidt, G. Diaz, M. Giacca and Y. Talmon, *J. Phys. Chem. B*, 2010, **114**, 3518–3525.
15 M. Carboni, A. M. Falchi, S. Lampis, C. Sinico, M. L. Manca, J. Schmidt, Y. Talmon, S. Murgia and M. Monduzzi, *Adv. Healthcare Mater.*, 2012, DOI: 10.1002/adhm.201200302.
16 G. Pabst, *Biophys. Rev. Lett.*, 2006, **1**, 57–84.

17 G. Pabst, J. Katsaras, V. A. Raghunathan and M. Rappolt, *Langmuir*, 2003, **19**, 1716–1722.
18 B. Simons and M. Cates, *J. Phys. II*, 1992, **2**, 1439–1451.
19 K. H. De Haas, C. Blom, D. Van den Ende, M. H. G. Duits, B. Haveman and J. Mellema, *Langmuir*, 1997, **13**, 6658–6668.
20 H. Hoffmann, U. Munkert, C. Thunig and M. Valiente, *J. Colloid Interface Sci.*, 1994, **163**, 217–228.
21 M. Gradzielski, *Curr. Opin. Colloid Interface Sci.*, 2011, **16**, 13–17.
22 M. Bergmeier, M. Gradzielski, H. Hoffmann and K. Mortensen, *J. Phys. Chem. B*, 1998, **102**, 2837–2840.
23 H. A. Barnes, *A Handbook of Elementary Rheology*, Institute of Non-Newtonian Fluid Mechanics, University of Wales Aberystwyth, 2000.
24 M. M. Cross, *J. Colloid Sci.*, 1965, **20**, 417–437.
25 P. N. Pusey and W. van Megen, *Nature*, 1986, **320**, 340–342.
26 R. G. Larson, *The Structure and Rheology of Complex Fluids*, Oxford University Press, New York, 1999.
27 K. A. Dawson, *Curr. Opin. Colloid Interface Sci.*, 2002, **7**, 218–227.
28 V. Trappe and P. Sandkühler, *Curr. Opin. Colloid Interface Sci.*, 2004, **8**, 494–500.
29 B. Van der Vorst, D. Van den Ende and J. Mellema, *J. Rheol.*, 1995, **39**, 1183–1200.
30 M. F. Brown, R. L. Thurmond, S. W. Dodd, D. Otten and K. Beyer, *J. Am. Chem. Soc.*, 2002, **124**, 8471–8484.
31 J. Pan, S. Tristram-Nagle, N. Kučerka and J. F. Nagle, *Biophys. J.*, 2008, **94**, 117–124.
32 R. Zhang, R. M. Suter and J. F. Nagle, *Phys. Rev. E: Stat. Phys., Plasmas, Fluids, Relat. Interdiscip. Top.*, 1994, **50**, 5047–5060.

